JOURNAL OF MATERIALS SCIENCE **37** (2002) 2825 – 2833

Diffusion bonding of TI-6AL-4V to AISI 316L stainless steel: mechanical resistance and interface microstructure

M. FERRANTE, E. V. PIGORETTI
Universidade Federal de São Carlos, Departamento de Engenharia de Materiais, 13560-905, São Carlos, Brasil

The interface microstructure and mechanical strength of joints obtained by diffusion bonding of alloy Ti-6A1-4V to AISI 316L stainless steel are presented. Bonding took place at 850, 900 and 950°C, maintained for different lengths of time (60 to 180 min). The highest recorded shear strength was equal to 382 MPa and was displayed by the specimen bonded at 950°C/180 min. Three different fracture paths were identified, each correlated to a characteristic strength range. From microprobe measurements and x-ray diffraction studies the following interface reaction products were identified: σ phase, α-Ti, Fe_2Ti, β-Ti and Fe-Ti. The interface growth kinetics obeyed a quadratic law, indicating diffusion controlled growth of the β-Ti layer. Finally, from correlations identified between β-Ti layer thickness and shear strength variations, some hypotheses on the role of both pores and interface reaction product on mechanical strength were presented.

1. Introduction

The joining of titanium and its alloys, either to themselves or to other materials, is becoming an important technology in the aerospace and chemical industries. Moreover, the low wear resistance of titanium alloys [1] can be obviated by their association with more suitable materials. As a rule, diffusion bonding is one of the first choices when dissimilar materials are concerned, and with superplastic materials such as titanium alloys this process is particularly efficient. Generally, current theories of diffusion bonding recognise two main mechanisms: (i) plastic deformation of the surface hills and valleys, thus creating an array of small interfacial voids and; (ii) mass transport to the voids by mechanisms similar to those acting in solid state sintering. The relative importance of (i) and (ii) depends on process parameters (temperature, pressure) and microstructural features such as grain size. On this respect, Hill and Wallace developed maps in which the various mechanisms are laid out in the space: *process variables* (homologous temperature, for instance) against *fractional bonded area*. [2]. The predictions of these maps were validated by those authors for a number of systems, such as Cu/Cu, α-Fe/α-Fe, γ-Fe/γ-Fe and 316 steel. According to this formalism, most of the time mass transport plays the dominant role in the bonding process. On the other hand, Kaibyshev *et al.* took the opposite view, emphasising the role of deformation processes such as superplastic flow [3], but clearly the model is restricted to materials exhibiting superplasticity. Similarly, Pilling and co-workers treated diffusion bonding as a special case of diffusive creep [4].

Besides mechanisms and kinetics, mechanical properties and interface features have been intensively investigated. Normally, when joining identical materials bond strength reaches that of the parent metal. For instance, Wang *et al*. measured values of shear resistance close to 620 MPa on diffusion bonded samples of a Ti alloy whose strength was 640 MPa [5]. Another investigation regarding Ti-4.5 Al-3Mo-1V diffusion bonded to itself, reported interface shear strength equal to 560 MPa [3]. However, when dissimilar materials are employed strength decreases due to residual stresses and to the formation of interfacial reaction products. As for interface characterisation, the most complete set of data on microstructure and interface reaction products was obtained by Alemán *et al*. on the system AISI 316L/Ti6242 (Ti5.5Al-1.8Mo-1.8Sn-3.6Zr) [6]. Important features are an interfacial layer of β-Ti, a number of Ti-Fe-Cr intermetallics, and the presence of sigma phase, all of them compatible with the Ti-Fe-Cr equilibrium diagram.

2. Experimental

2.1. Materials

The base materials are 3 mm thick plates of Ti-6Al-4V and AISI 316L stainless steel. The plates were cut into rectangles 40×10 mm^2, the surfaces to be bonded were finished by grinding up to #1200 emery paper and washed in an alcaline solution. This was followed by ultrasonic cleaning in acetone during 20 min and hot air drying.

2.2. Diffusion bonding

Part of the equipment and the sample geometry are shown in Fig. 1a. All bonding experiments were performed in a vacuum better than 5×10^{-5} Torr; a mechanical pressure equal to 8 MPa was applied to the overlapping area of the sample and the time-temperature parameters employed were:

$$T(^{\circ}\mathrm{C}) : 850\text{–}900\text{–}950^{\circ}\mathrm{C};$$
$$t(\mathrm{min}) : 60\text{–}90\text{–}120\text{–}150\text{–}180$$

giving 15 different conditions. An average of 8 samples were produced for each condition. Heating and cooling rates were equal to 50 and 20°C min^{-1}, respectively; during some of the bonding experiments the deformation rate of the sample was measured using a linear variable displacement transducer (LVDT).

2.3. Mechanical tests, metallography and structural studies

Samples were tested in shear at room temperature, see experimental arrangement in Fig. 1b. Load was applied in compression at 0.5 mm min^{-1}. The interface region was examined by optical and scanning electron microscopy (SEM). Quantitative EDS microanalysis and Vickers microhardness measurements across the interface were also performed and x-ray spectra were obtained on fracture surfaces using Cu-K_α radiation.

3. Results

3.1. Shear strength

Table I summarises the shear strength values obtained from 102 specimens. These and their fracture modes were respectively identified and classified as follow:

Specimens: the initial three numbers indicate the bonding temperature whilst the other three correspond to the bonding time. Letters identify the individual specimens obtained under identical temperature/time conditions. Thus, 850060C identifies the third specimen obtained at 850°C/60 min.

Fracture mode: $0 \Rightarrow$ non-bonded specimen or specimen broken during test preparation;

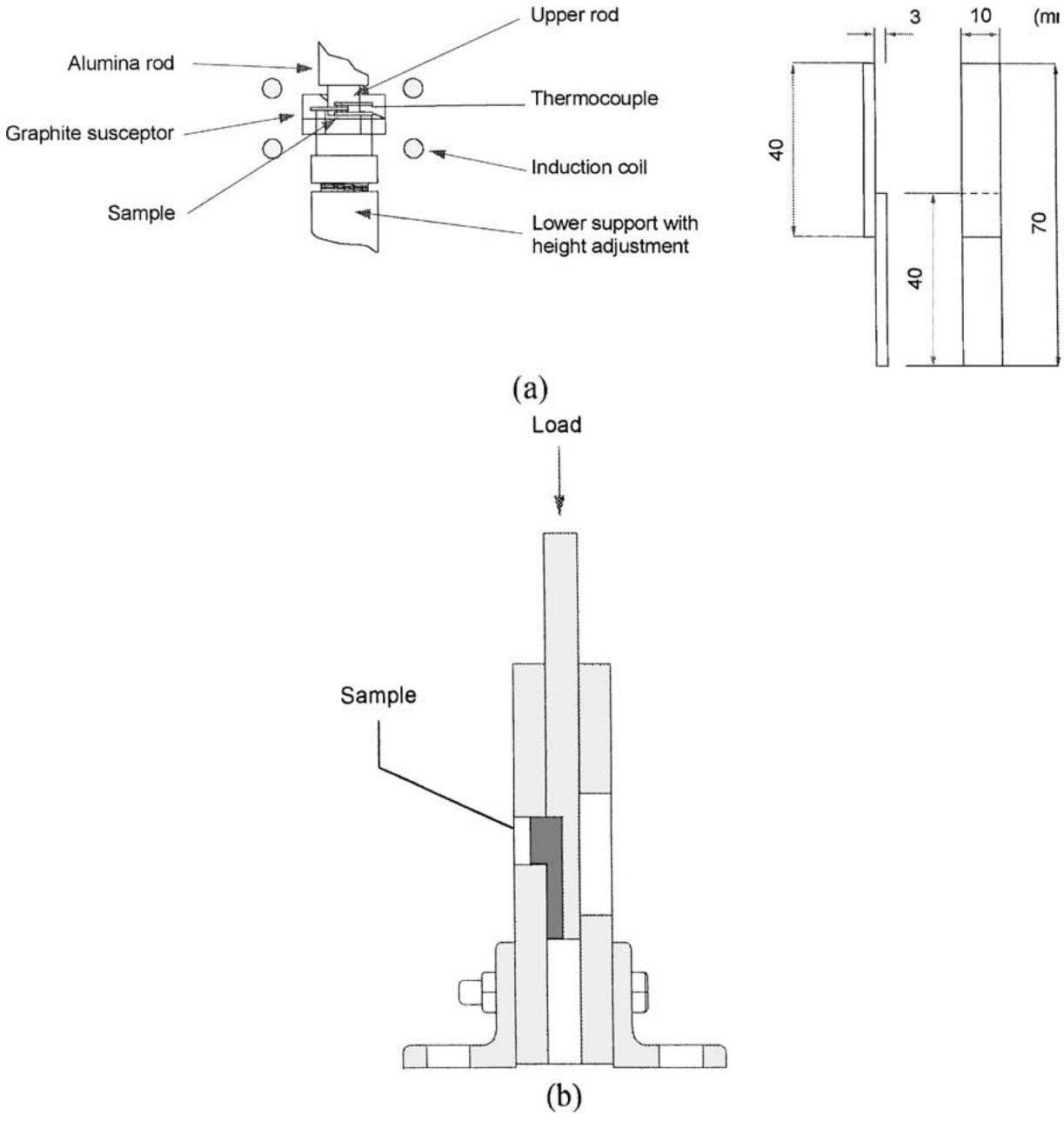

Figure 1 Schematic of the diffusion bonding rig and of the shear specimen geometry (a). Shear testing system (b).

TABLE I Results of the compression shear tests and description of the respective fracture mode

Sample	τ (MPa)	Fracture mode	Sample	τ (MPa)	Fracture mode	Sample	τ (MPa)	Fracture mode
850060A	68	1	900060D	201	1	950060B	335	3
850060B	98	1	900060E	260	2	950060C	292	3
850060C	223	2	900060F	256	2	950060D	328	3
850060D	245	2	900060G	232	2	950060E	–	0
850060E	207	2	900060H	260	2	950060F	273	3
850060F	254	2	900090A	270	2	950060G	286	3
850090A	175	1	900090B	236	1	950090A	320	3
850090B	220	1	900090C	250	1	950090B	342	3
850090C	98	1	900090D	281	3	950090C	352	3
850090D	109	1	900090E	230	1	950090D	275	3
850090E	215	2	900090F	254	2	950090E	321	3
850090F	270	3	900090G	256	2	950090F	303	3
850120A	241	2	900120A	229	1	950090G	270	3
850120B	147	1	900120B	229	2	950120A	344	3
850120C	255	3	900120C	307	3	950120B	321	3
850120D	134	1	900120D	324	3	950120C	–	0
850120E	236	2	900120E	334	3	950120D	289	1
850120F	251	2	900120F	274	2	950120E	331	3
850150A	262	2	900120G	280	2	950120F	288	3
850150B	274	2	900150A	281	2	950120G	319	3
850150C	272	3	900150B	283	3	950120H	309	3
850150D	273	3	900150C	360	3	950150A	306	1
850150E	253	3	900150D	280	1	950150B	186	1
850150F	266	2	900150E	284	1	950150C	307	2
850180A	201	2	900150F	284	3	950150D	350	3
850180B	289	3	900150G	296	2	950150E	325	2
850180C	269	2	900180A	172	1	950150F	312	2
850180D	215	2	900180B	250	2	950180A	348	3
850180E	293	2	900180C	352	3	950180B	251	1
850180F	279	3	900180D	298	3	950180C	321	3
850180G	234	2	900180E	211	1	950180D	285	3
900060A	267	2	900180F	382	3	950180E	283	2
900060B	275	3	900180G	280	3	950180F	263	1
900060C	190	2	950060A	322	1			

Samples tested: 102.

1 ⇒ Fracture running along the interface;

2 ⇒ Fracture running within the Ti alloy, with partial exfoliation;

3 ⇒ Fracture running within the Ti alloy with total exfoliation.

Some typical fracture surfaces are shown in Fig. 2.

In order to check for relationships between strength and bonding time, additional samples were produced at 950°C employing both very short (10, 12, 15, 20, 30 min) and long bonding times (210, 240, 270 min). Shear test were performed and the results were placed alongside the already existing data for the same bonding temperature (Table I). Fig. 3 summarises the complete set of results for the 950°C sample and it is apparent that strength is lower at both very short and very long bonding times. An important observation is that shear strength and fracture mode are related; for instance, specimens having less than 200 MPa shear strength tend to exhibit fracture mode 1, that is, crack running along the original interface, whilst for high strength mode 3 dominates. These correlations are shown in Fig. 4, as frequency of each fracture mode against shear strength.

3.2. Interface microstructure

Fig. 5 is a SEM micrograph of a typical bond interface. Numbers below identify microstructural features on which the EDS microprobe measurements were performed. The complete set of results of such measurements is summarised in Table II. Three regions can be recognised in Fig. 5:

TABLE II EDS Microanalysis results of a 900°C/150 min diffusion bonded sample (wt%)

Point	Fe	Ti	Cr	Ni
0	69.5	0.6	15.0	11.0
1	56.7	8.5	24.7	3.4
2	51.0	18.0	24.0	3.2
3	42.0	45.0	3.5	4.9
4	14.0	78.4	2.0	1.3
5	9.8	80.5	0.9	1.3
6	6.4	82.4	0.6	1.3
7	6.2	84.0	0.4	1.3
8 [8a]	6.0 [7.1]	86.7 [85.5]	0.7 [1.0]	1.0 [0.9]
9 [9a]	2.2 [6.2]	91.5 [86.6]	0 [0.7]	0.4 [0.9]
10 [10a]	6.4 [4.3]	87.0 [89.2]	0.2 [0]	1.2 [0.7]
11 [11a]	5.2 [2.0]	87.8 [91.6]	0 [0]	1.4 [0.5]

Numbers correspond to regions identified in Fig. 5.

(i) A ∼3 μm thick layer adjacent to the steel which will be denominated *interface layer*, comprising points 1, 2 and 3.

(ii) Moving to the left there is a 10 to 40 μm thick layer, here called *β-Ti transformed region*, comprising points 4 to 7. Thickness is a function of

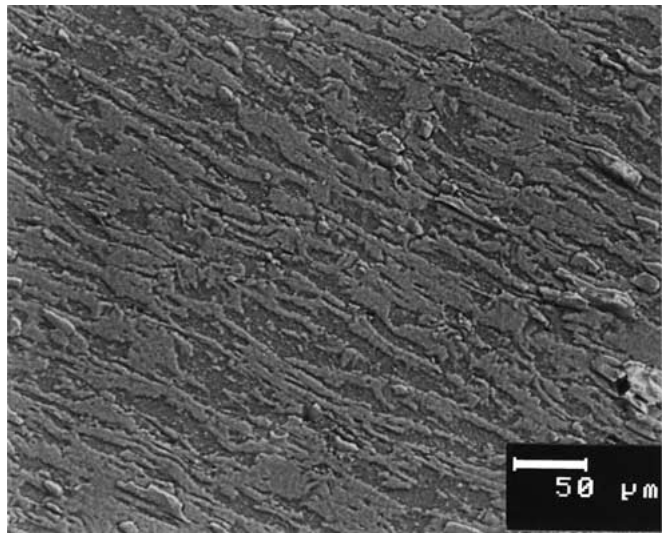

(a)

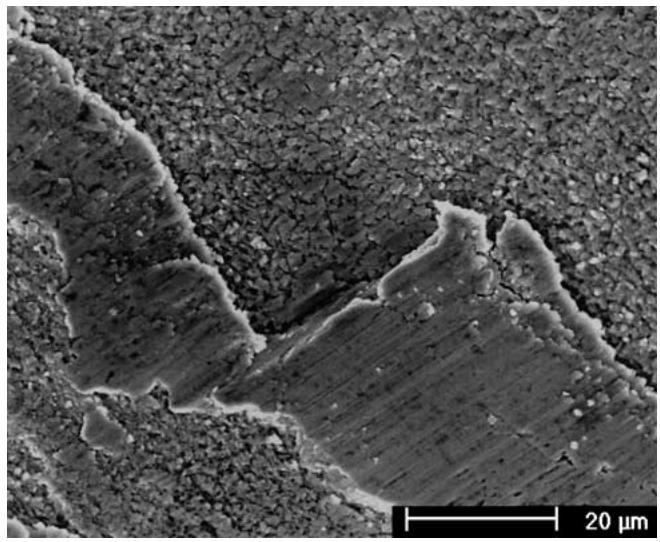

(b)

Figure 2 Typical fracture surfaces after shear testing: (a) sample bonded at 850°C/90 min, steel side, shear strength equal to 200 MPa; (b) sample bonded at 950°C/150 min, Ti alloy side, shear strength equal to 300 MPa. Strength given are average values for the correspondent experimental conditions.

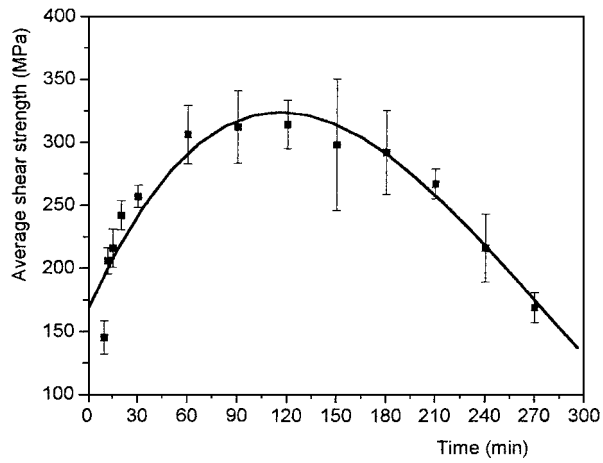

Figure 3 Shear strength as a function of bonding time, for specimens diffusion bonded at 950°C.

bonding time which varied between 60 and 180 min, respectively.

(iii) Adjacent to the Ti alloy a region exhibiting Widmanstätten morphology, here called *acicular region*, extends from point 8 to point 11. Thickness varies between 35 and 165 μm depending on bonding time.

For the 950°C/150 min sample, Fig. 6 shows concentration profiles of a number of elements across the interface. It is apparent that diffusion of Fe into the Ti alloy is much faster than the opposite, that is, Ti into the steel. Also, a Cr-rich region can be observed close to the interface, steel side. Compositional data were combined with x-ray diffraction measurements taken on fracture surfaces and the following interfacial reaction products were thus identified:

$$\sigma \text{ phase; } \alpha\text{-Ti; } Fe_2Ti; \beta\text{-Ti; FeTi}$$

These results were essentially confirmed by earlier and by recent transmission electron microscope observations [6, 7].

3.3. Interface growth kinetics

From plots of log thickness of the β-transformed region against the log of bonding time a slope equal to 1/2 was obtained. Fig. 7 is a plot of the β-Ti transformed region

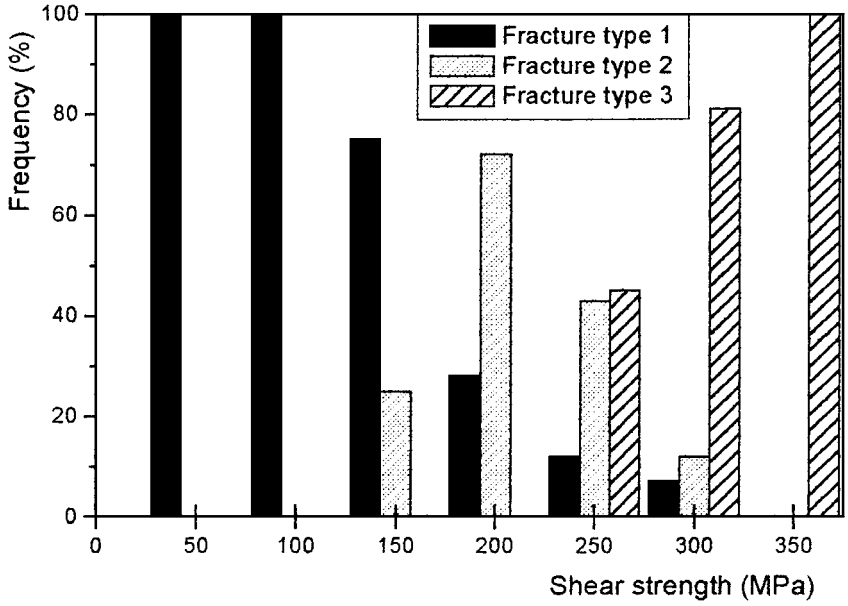

Figure 4 Correlation between the frequency of different fracture modes (1, 2 and 3) with the correspondent shear strength.

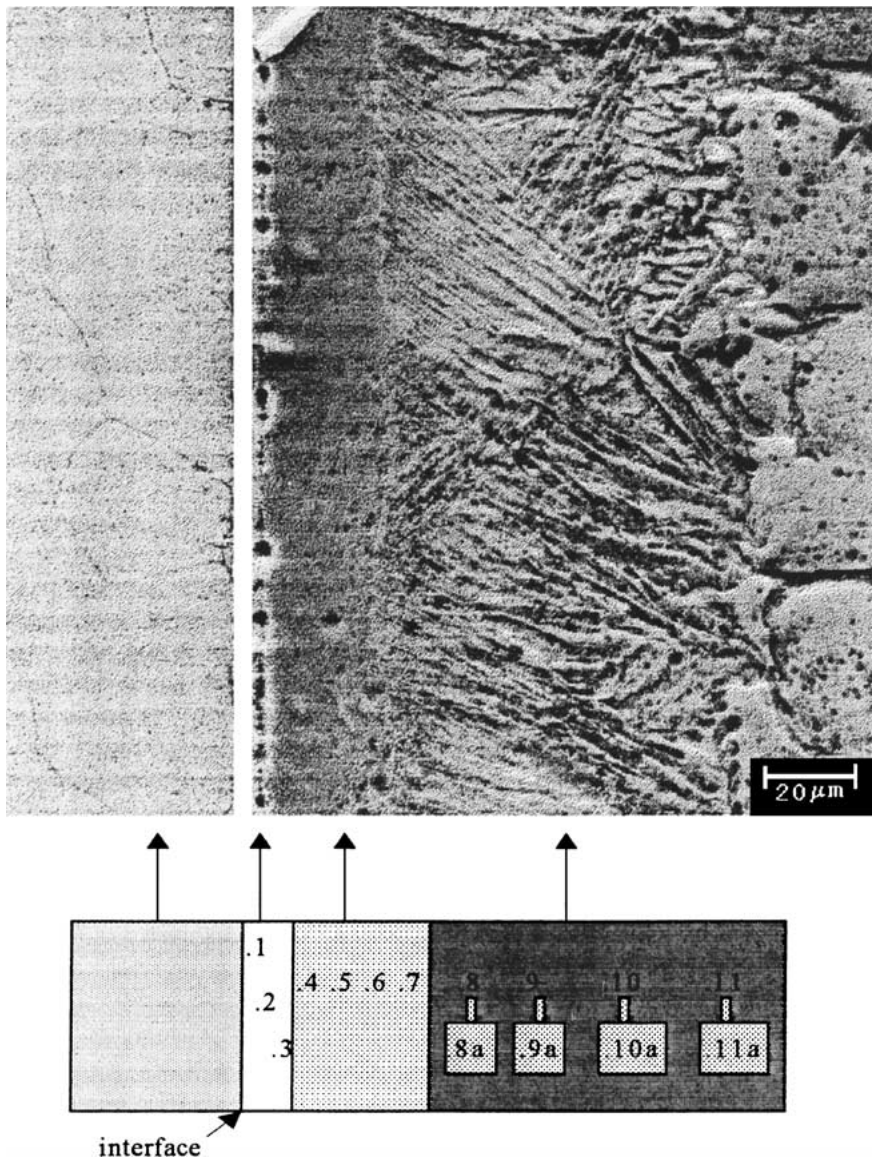

Figure 5 Microstructure of a Ti/304 stainless steel interface produced at 950°C/150 min. Numbers identify positions on which microprobe elemental analysis was performed, see text for details. The microstructural features here depicted are typical of all experimental conditions.

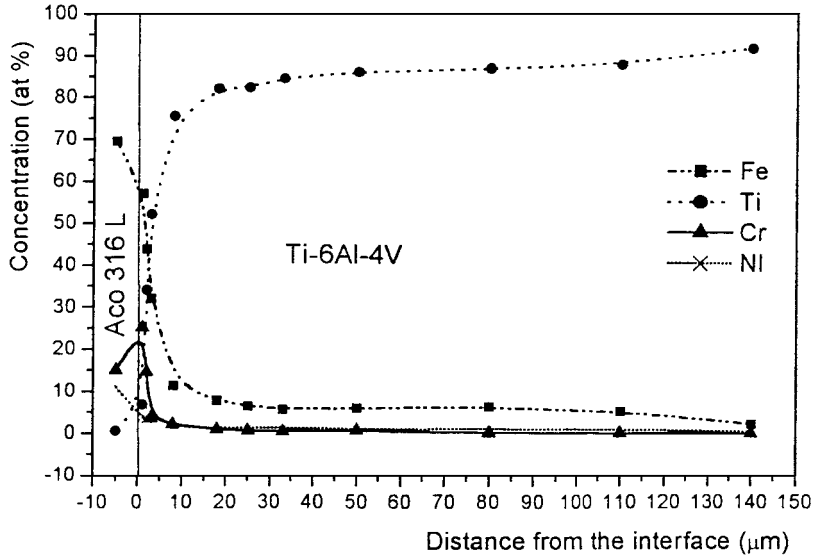

Figure 6 Concentration profiles of Ti, Fe, Cr and Ni, measured across the Ti/304 interface shown in Fig. 5.

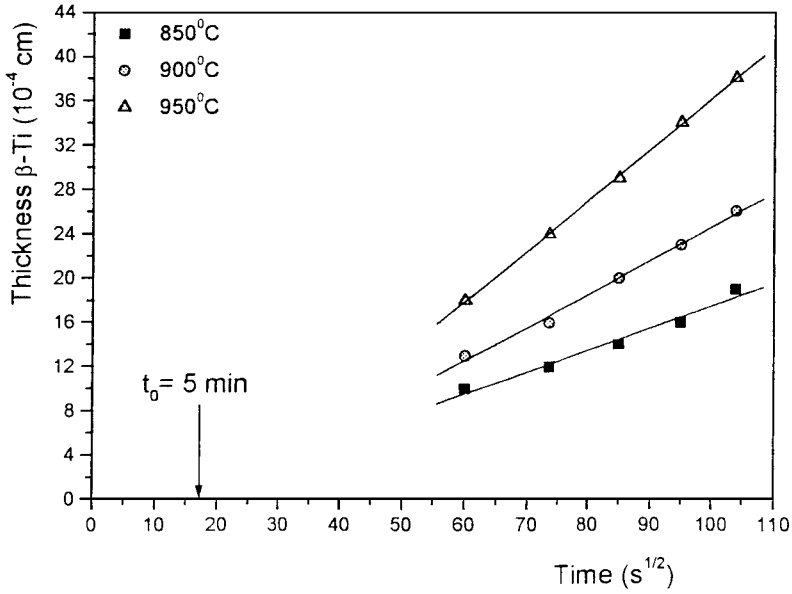

Figure 7 Evolution of the β-Ti transformed region with the square root of bonding time, at three bonding temperatures.

thickness against the square root of time, for the three bonding temperatures here employed; straight lines can be drawn along the experimental points indicating diffusion controlled growth kinetics of the β-Ti layer.

4. Discussion

The bonding condition giving the maximum shear strength, that is, 382 MPa, was 950°C/180 min. A general conclusion regarding the mechanical behaviour of the joints is summarised in Fig. 8, which shows that irrespective of bonding temperature shear strength is lower for both short and long bonding times. Therefore, the observation that fracture along the interface is correlated with low resistance and with low bonding time, plus the detection of pores along the correspondent fracture surfaces, see Fig. 2, indicates that these defects control the shear strength and it can be concluded that some degree of interface porosity existed up to 120 min bonding time for joints obtained at 850 and 900°C and up to 90 min for the 950°C samples. As for the decrease of mechanical strength for bonding times longer than

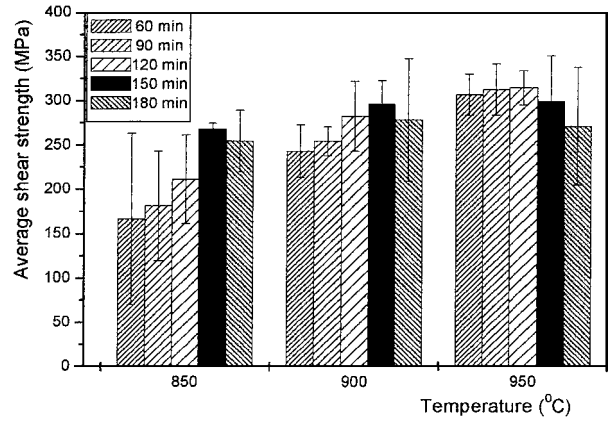

Figure 8 Shear strength at three bonding temperatures as a function of bonding time.

180 min, it can be assumed that failure takes place by the presence of increasingly thick brittle reaction products, sigma phase for instance. In these experimental conditions the crack path is highly irregular as Fig. 2 showed

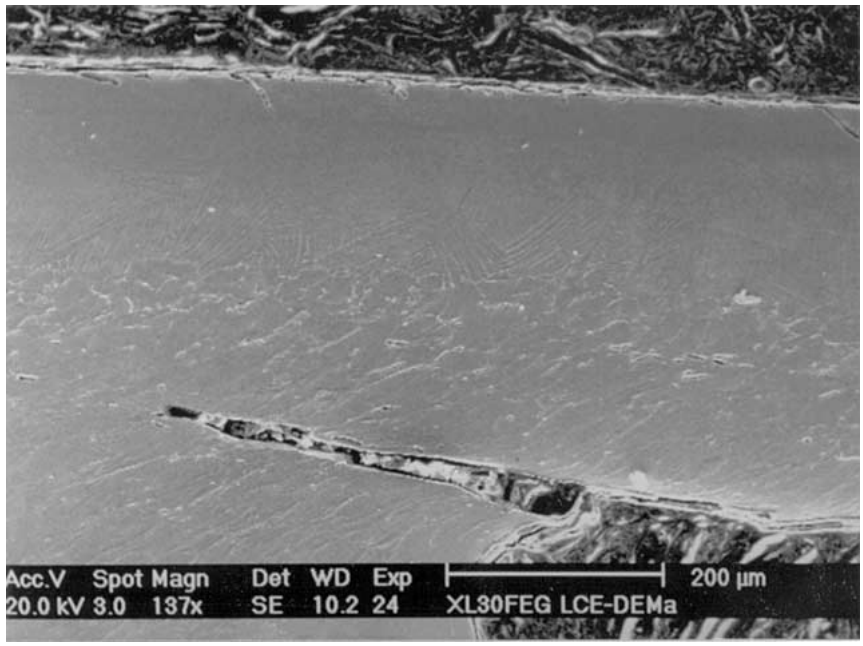

Figure 9 Profile of a fracture path typical of high shear strength samples, viewed on a plane normal to the bonded interface.

and microanalysis measurements performed on its surface gave the results summarised in Table II. This data indicates that the crack is running through phase χ or σ (point 1), then through phases σ, (χ), Fe-Ti, Fe_2Ti and the initial part of the β-Ti layer (points 2 and 3). It must be recalled that all these phases are brittle, particularly σ. Also, it was observed that fracture mode 3 characterises joints with optimal strength and Fig. 9 shows the profile of a typical fracture path of one of such samples (900°C/150 min, 309 MPa). It can be seen that the crack runs parallel to the interface, keeping from it a distance between 300 and 400 μm and that its path is associated with heavy plastic deformation. Vickers microhardness measurements taken across the interface and into the Ti alloy showed that after 180 min bonding time, the hardness close to the interface reached 600 kgf mm^{-2}. This value is progressively reduced to 225 kgf mm^{-2} (base metal characteristic hardness) at about 300 μm from the interface and stabilises at that level. Therefore, the crack shown in Fig. 9 runs close to the base metal, in other words it is a high-energy ductile fracture propagating within non-hardened material. With regard to the above discussion on intermetallic phases and their influence on shear strength it must be recalled that a common occurrence when Ti and steel are diffusion bonded is the formation of TiC, a finely dispersed phase which causes substantial embrittlement. This carbide was not detected in the present study in which the metallographic observation was carried out at SEM resolution, but a recent paper by Kliauga *et al*. [7] reports the presence of TiC in a diffusion bonded Al_2O_3/Ti interlayer/AISI joint. Typical dimension are 200 nm and the carbide is located close to the Ti/steel interface (Ti side). Interlayers are also frequently employed in metal/metal diffusion bonding as a diffusion barrier, with mixed results as far as mechanical strength is concerned. For instance, Church and Wild tested a number of different interlayers between Ti-6Al-4V and two Ni-Cr steels [8] but compressive shear strength decreased when compared with that of joints produced without interlayers. On the other hand, Wisbey and Ward-Close performed diffusion bonding experiments using Ti alloy and INCONEL and found a significant enhancement of shear strength when a combination of Ta and Ni interlayers was employed [9]. In all cases the nature of the reaction products changed substantially in the presence of interlayers.

As for the interface growth kinetics Fig. 7 showed that it is diffusion controlled, and logarithmic plots of the rate constant against $1/T$ gave an activation energy (Q) and a frequency factor (D_o) equal to 195 kJ mol^{-1} and 0.5 cm^2 s^{-1}, respectively. Recent literature data regarding values of interdiffusion activation energies for Ti/AISI304 steel [10] shows that Q is strongly dependent on the chemical composition, see below:

Ti (at%)	50	60	70	80	90
Q (kJ mol^{-1})	80.8	78.9	97.8	179.5	185.2

Comparing data it can be seen that at the early stages of reaction the activation energy for layer growth is somewhat higher than the activation energy for Fe interdiffusion. These quantities become essentially equal when planes further away from the interface are considered. Thus, it can be supposed that the initially, bonding took place with some measure of interface control.

Another interesting feature of Fig. 7 is the time intercept t_o, equal to approximately 150–400 s, which can be considered equivalent to an incubation time for the β-transformed layer formation. It can be assumed that t_o corresponds to the time during which plastic deformation of the surface hills and valleys takes place. This assumption is supported by data on the deformation rate of the samples, see Fig. 10, which shows a typical graph of change of thickness against bonding time. This

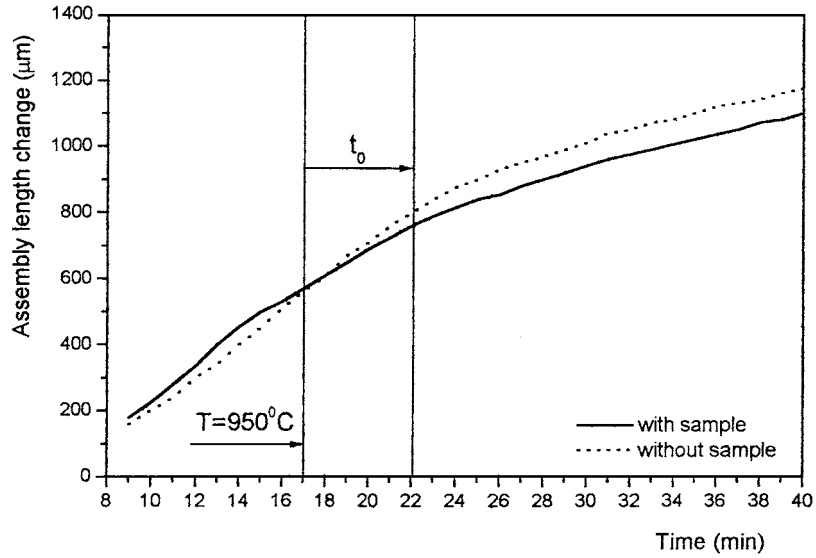

Figure 10 Deformation rate of the sample given by comparing the change of thickness of the sample plus static loading system with the change of thickness of the loading system alone.

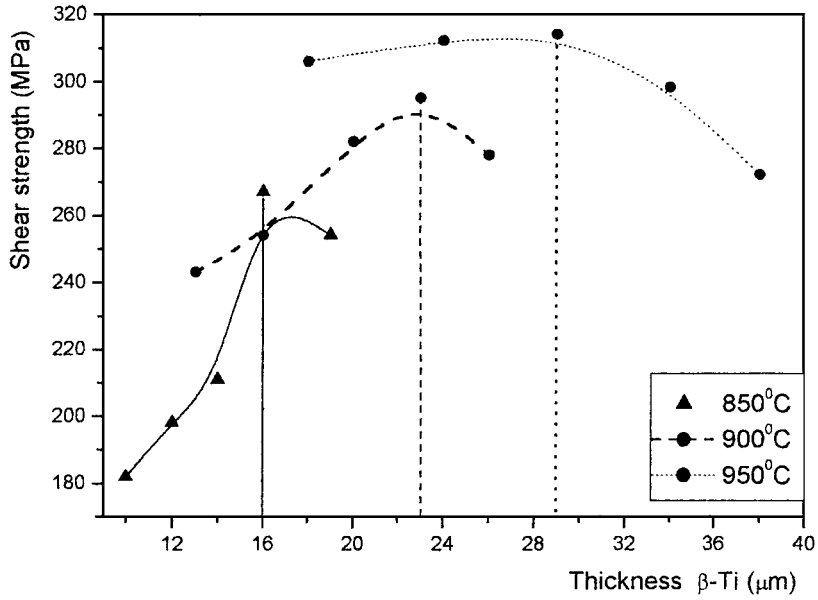

Figure 11 Correlation between shear strength and β-Ti transformed region, showing the existence of a critical thickness beyond which the shear strength decreases from its maximum value.

experiment employed a LVDT measuring the displacement of the rod which transmits to the sample the static load applied during the bonding operation, in other words, the sample deformation along the vertical direction. For each bonding temperature two set of data were acquired: (i) thermal expansion of the assembly with the sample, and (ii) thermal expansion of the assembly without the sample. As Fig. 10 shows, initially curve (i) is above curve (ii), the difference corresponding to the sample expansion. However, once reached bonding temperature ($t = 9$ min) the two curves approach and superimpose, indicating that the former assembly expands at a lesser rate than the latter, in other words its thickness is progressively reduced by the plastic deformation of surface hills and valleys. This phenomenon lasts about 7 min (400 s) which can be interpreted as the time employed by the deformation processes referred to above and in the Introduction, since this length of time is close to t_o obtained from Fig. 7. From the above discussion it can be concluded that plastic deformation is a reasonably fast process and that most of the bonding time is taken up by diffusional mechanisms.

Finally, a correlation between mechanical strength, interface characteristics and the interplay of bonding mechanisms is contained in Fig. 11, a plot of shear strength against the β-transformed zone thickness for the three bonding temperatures. From the graph it is apparent that for each temperature a critical thickness exists, beyond which shear strength decreases from its maximum value. Also, the lower the bonding temperature the steeper the curve of strength against β-transformed zone thickness. On this respect, from Fig. 7 it can be calculated that the time intervals to reach critical thickness are 150, 120 and 80 min, at 850, 900 and 950°C, respectively. Thus it can be calculated that the rate of strength increment grows with bonding temperature and it can be concluded that this velocity is related to the rate of elimination of interfacial porosity.

As for the dependence of critical thickness with bonding temperature, a possible interpretation would be that interfacial pores act as stress concentrators.

5. Conclusions

1. Regardless of bonding temperature shear strength shows a maximum at some intermediate bonding time. The highest recorded value was 382 MPa, displayed by the specimen bonded at 950°C/180 min.

2. Low strength specimens tend to fracture mainly along or very close to the bonding interface; the crack runs through the brittle phases, viz., σ, χ, FeTi, Fe_2Ti and the initial part of the β-Ti layer. These phases were identified by microprobe analysis and x-ray diffraction. For high strength bonds the fracture propagates within the Ti alloy at a distance of 300–400 μm from the interface.

3. Plastic deformation, leading to the smoothing out of surface hills and valleys is a fast process lasting typically 7 min.

4. A critical thickness of the β-transformed zone exists, beyond which shear strength decreases from its maximum value. It can be concluded that before this maximum, bond strength is controlled by the interfacial porosity and after it by the presence of brittle reaction products. The observation that critical thickness increases with temperature (hence with the efficiency of pore elimination) indicates that interfacial pores act as stress concentrators.

References

1. K. G. BUDINSKY, *Wear* **151** (1991) 203.
2. A. HILL and E. R. WALLACH, *Acta Metall.* **9** (1989) 2345.
3. O. A. KAIBYSHEV, Y. YA. LUTFULLIN and V. K. BERDIN, *ibid.* **42** (1994) 2609.
4. J. PILLING, D. W. LIVESSEY, J. AWKYARD and N. RIDLEY, *Metal Sci.* **3** (1987) 117.
5. Z. C. WANG, N. RIDLEY, G. W. LORIMER, D. KNAUSS and G. A. D. BRIGGS, *J. Mater Sci.* **31** (1996) 5199.
6. B. ALEMÁN, I. GUTIERREZ and J. J. URCOLA, *Mat. Sci. Technology* **9** (1993) 633.
7. A. M. KLIAUGA, D. TRAVESSA and M. FERRANTE, *Materials Characterization* **46** (2001) 65.
8. S. C. CHURCH and R. K. WILD, *J. Vac. Sci. Technol.* A **16** (1988) 1885.
9. A. WISBEY and C. M. WARD-CLOSE, *Mater. Lett.* **21** (1994) 47.
10. G. B. KALE, R. V. PAITL and P. S. GAWADE, *Journal of Nuclear Materials* **257** (1999) 44.

Received 12 December 2000
and accepted 13 February 2002